CHAPTER SEVEN

Inhibition of Homogeneous Formation of Calcium Oxalate

This chapter is based on work published in two papers

A. D. Wallace, A. Al-Hamzah, C. P. East, W. O. S. Doherty and C. M. Fellows, "Effect of Poly(acrylic acid) End-group Functionality on Inhibition of Calcium Oxalate Crystal Growth" *J. Appl. Polym. Sci.*, 116(2), 1165-1171 (2010).

C. P. East, A. D. Wallace, A. Al-Hamzah, W. O. S. Doherty and C. M. Fellows, "Effect of Poly(acrylic acid) Molecular Mass and End-group Functionality on Calcium Oxalate Crystal Morphology and Growth" *J. Appl. Polym. Sci.*, 115(4), 2127-2135 (2010).

7.1 Introduction

Poly(acrylic acid) (PAA) and poly(maleic acid) are used for scale control in the sugar industry.[1-4] The exact mechanism by which these polymers function is still poorly understood, but several mechanisms may plausibly play a role: chelation of calcium ions by PAA, specific adsorption of PAA to active sites on the surface of crystallites to retard growth or alter crystal habit, electrostatic stabilization of calcium oxalate crystallites by PAA, and nucleation of calcium oxalate crystallites by Ca^{2+}: PAA complexes. Current research in modifiers of crystal growth and habit, points towards selective adsorption of the additive at the crystal/solution interface as the dominant mechanism of crystal action.[1, 5]

The main aim of this chapter is to determine the efficiency of PAA with different end-groups and controlled molecular mass in the range 1400-17000 g/mol as scale inhibitors to prevent CaC_2O_4 crystallization in the bulk solution at room and elevated temperatures using conductivity and turbidity measurements. A further aim was interpreting the results in term of the mechanism already suggested for inhibition of calcium carbonate.

7.2 Experimental determination of conductivity and turbidity at 23 °C

Two solutions, 0.137 M (12056 ppm) of $C_2O_4^{2-}$ as $Na_2C_2O_4$ and 0.137 M (5480 ppm) of Ca^{2+} as $CaCl_2$ were prepared. These solutions and the R/O water used were filtered and degassed using a 0.45 μm Millipore solvent filter. PAA solutions were prepared as 0.015 g in 20 mL water and used after 3 days.

Filtered (0.45μm cellulose acetate membrane) deionized water (246 mL) was placed in a 500 mL cleaned beaker containing the conductivity probe. Under magnetic stirring, Ca^{2+} as $CaCl_2$ solution to give a final concentration of 22 ppm and scale inhibitor solution to give 6 ppm were added to the beaker. After equilibration (approximately 2 min), the photodetector in the

spectrophotometer were zeroed. The solution was pumped continuously through a 1 cm Quartz flow cell using a Gilson peristaltic pump (Minipuls 2) with 4mm silicon tubing and then returned to the main mixture. $C_2O_4^{2-}$ as $Na_2C_2O_4$ solution was added to the beaker to give a final concentration of 48 ppm and the recording of absorbance at 900 nm started 20 s later from the adding of $C_2O_4^{2-}$solution.

Analogue outputs from conductivity prop and spectrophotometer were digitally converted using a Picolog A/D Converter 16 (16 Bit) and Picolog recording software and data was acquired every 10 seconds. After each experiment all equipment was flushed multiple times with weak acid followed by R/O water.

7.2.1 Results and Discussion

The induction times by conductivity and turbidity measurements were determined in the absence and presence of PAAs at 23 °C. For those data, *t*-test and F-test were calculated to determine if there is any statistically significant different at confidence interval 95 % as well as the correlation coefficient as shown in Figure 7.1. The calculated *t* and F were 0.45 and 1.02 and their tabulated values at 21 freedoms are 2.08 and 2.10 respectively, which indicate there is no significant different between the inductions times by conductivity and turbidity measurements for CaC_2O_4 formation at 23°C (Steel & Torrie, 1980).[6]

Results obtained for induction times measured at 23°C by conductivity and turbidity are given in Table 7.1 and Figures 7.2 and 7.3. For all series, induction time was strongly dependent on molecular mass, with M_n = 2000-4000 showing the longest induction times as shown in Figures 7.4 and 7.5.

The overall trend in inhibition behaviour over both the induction and crystallization periods is consistent with a model where PAA operates by adsorption/desorption to active sites on the

growing calcium oxalate crystallites as suggested in Chapter 3. A molecular mass dependence on effectiveness is expected, as small chains will desorb rapidly while large chains will not relax sufficiently to cover the active site within the required timeframe, and this optimum mass of the polymer has been found to lie between 2000 and 4000 g/mol for PAA in a number of systems.[7] The distribution and spacing of the ions on different surfaces of the crystallites will also influence the degree to which PAA will adsorb: in COD, the {010} faces present mainly oxalate ions, while a dense pattern of calcium ions is presented at {100} faces, making PAA adsorption much more favorable to the latter.[8] Two separate influences of a hydrophobic end-group on adsorption/desorption may be postulated:

A hydrophobic end group may encourage desorption, as it provides a hydrophilic end group, not bound to the crystallite surface, from which desorption may begin. However, interactions between the hydrophobe and the aqueous phase are also unfavorable, so the presence of a hydrophobe will encourage the polymer to remain in an environment where polymer concentration is high enough that end-groups may self-associate to remove themselves from the aqueous phase. This trend would be expected to become more pronounced as the length of the end-group increases, possibly explaining the minimum in induction time and crystallization time at intermediate end-group sizes. Self-association of the CIB end-groups would be expected to be less probable than self-association of the HIB end-groups due to the more rigid structure and smaller surface area of the former, possibly explaining the poorer performance of CIB-terminated in comparison to HIB-terminated PAA.

The role of both hydrophilic and hydrophobic end-groups in modifying PAA would then be to encourage adhesion to growing crystallite surfaces, retarding growth and modifying crystal habit. As the self-assembly of hydrophobes in aqueous solution is entropically driven by the reduction of restrictions on the motion of water, the effectiveness of hydrophobes in

maintaining PAA adhesion to crystallite surfaces would be expected to increase, and accordingly a subset of the PAA prepared were investigated at 80 °C (Table 7.2).

Table 7.1- The induction times for CaC_2O_4 formation in the presence of PAA at 23 °C

End Groups of PAA	M_n	PDI	SS µS/cm	IT (s) by Abs.	IT (s) by Cond.
CMM	2106	1.3	-	1010	950
EIB	1669	1.3	175	491 +71 -12	487 +48 -94
	5065	1.3	172	134 +59 -159	129 +174 -158
	7180	1.3	170	163 +12 -2	168 +156 -137
CIB	1689	1.4	178	496 +54 -33	490 +108 -54
	3518	1.2	179	512 +232 -167	412 +267 -56
	6210	1.2	173	492 +83 -81	431 +127 -74
	8400	1.2	173	350 +127 -27	312 +155 -35
	10988	1.2	171	283 +134 -371	210 +151 -62
	13209	1.1	167	112 +8 -7	110 +8 -7
HIB	1403	-	176	485 +55 -33	466 +25 -36
	1981	1.2	180	561 +268 -52	567 +51 -94
	4224	1.2	174	580 +17 16	555 +113 -101
	6227	1.2	171	531 +6 -6	511 +164 -148
	8928	1.1	170	418 +51 -35	376 +64 -27

End Groups of PAA	M_n	PDI	SS µS/cm	IT (s) by Abs.		IT (s) by Cond.	
DIB	2422	1.3	180	553	+312 -420	322	+61 -22
	4472	1.3	179	947	+43 -66	842	+207 -37
	6203	1.5	180	679	+50 -36	669	+224 -155
HDIB	1687	-	174	396	+31 -2	395	+33 -5
	2767	-	177	559	-7 -69	571	+41 -86
	4135	-	173	928	+122 -309	981	+297 -108
	17167	-	167	213	+25 -18	213	+99 0

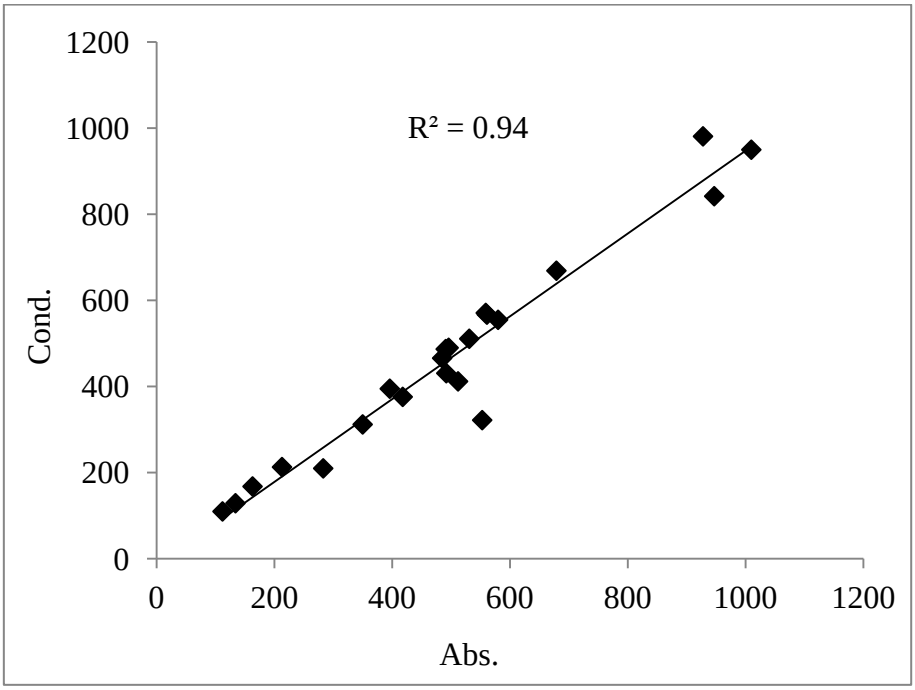

Figure 7.1- Induction times by conductivity versus induction times by turbidity for CaC_2O_4 formation at 23°C.

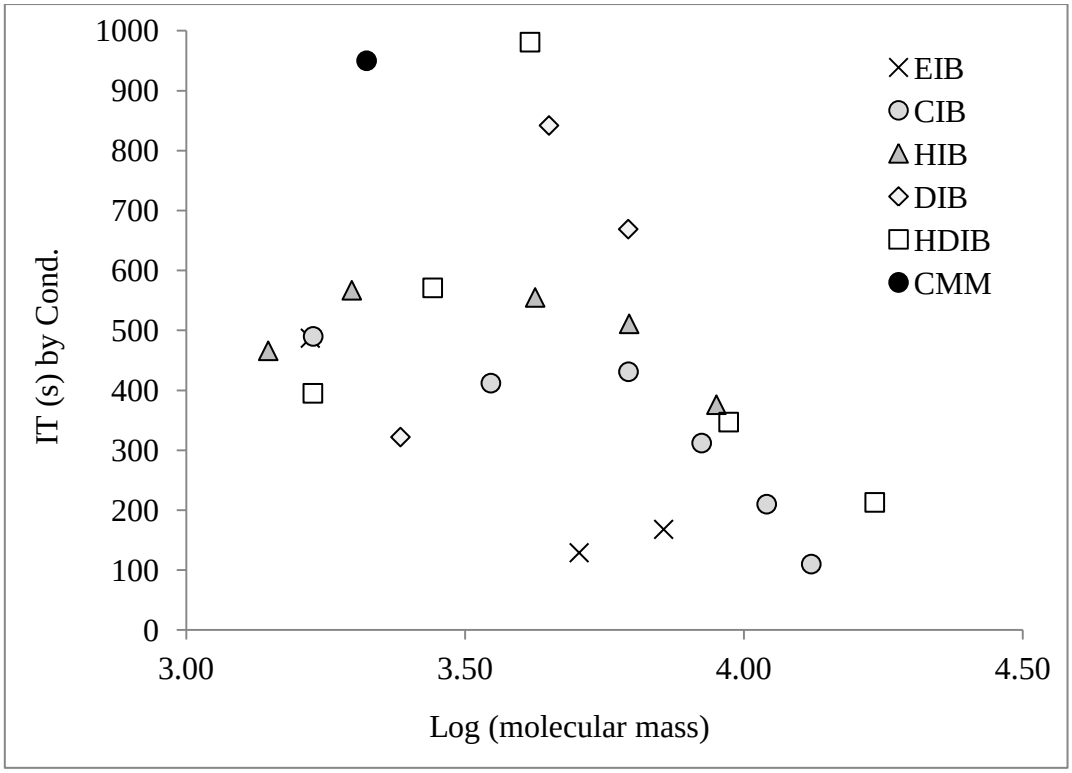

Figure 7.2- Induction times determined by conductivity for PAA terminated with EIB (×), HIB (▲), CIB (●), DIB (◊), HDB (□), and CMM (●) end-groups.

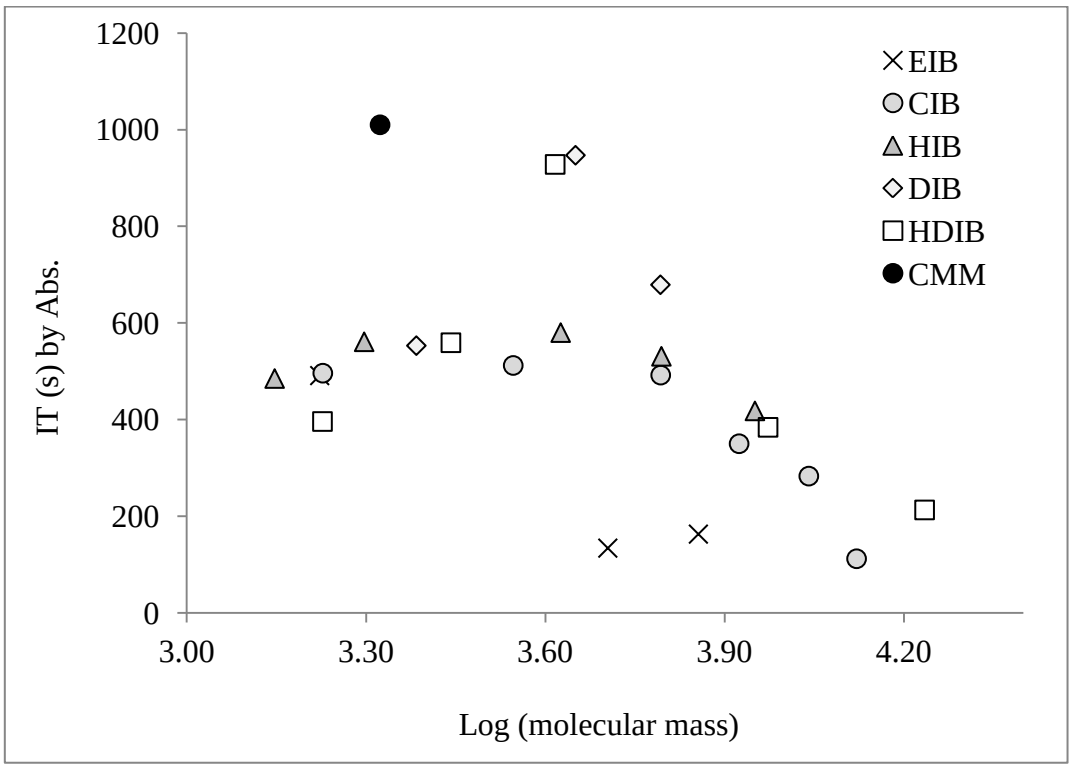

Figure 7.3- Induction times determined by turbidity for PAA terminated with EIB (×), HIB (▲), CIB (●), DIB (◊), HDB (□), and CMM (●) end-groups.

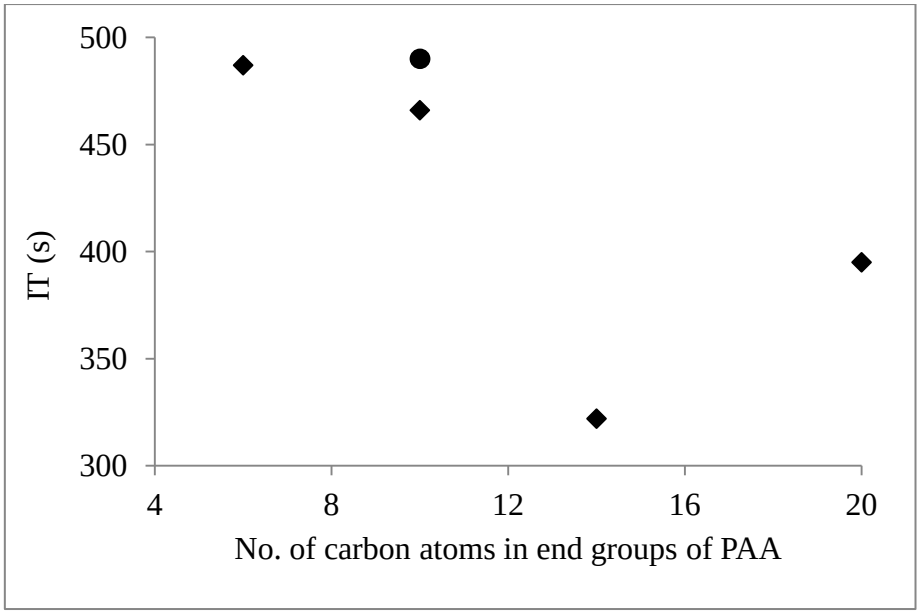

Figures 7.4- Induction times by conductivity of CaC_2O_4 formation on the presence of PAA with different end groups ($M_n \leq$ 2000) at 23°C. (● = CIB-PAA)

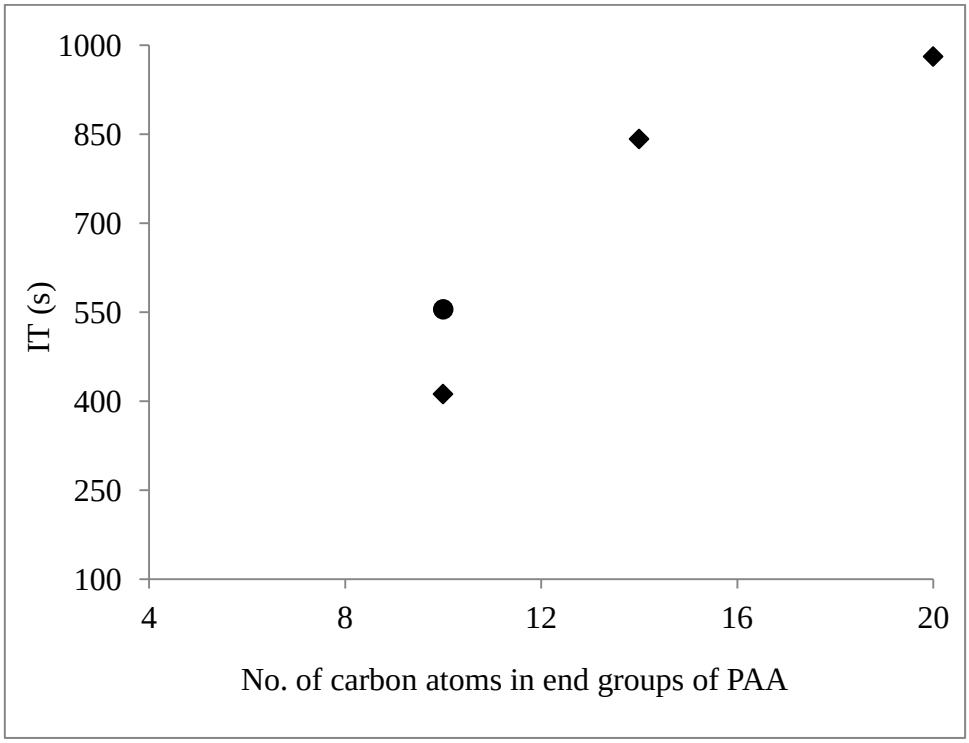

Figures 7.5- Induction times by conductivity of CaC_2O_4 formation on the presence of PAA with different end groups (2000 $\leq M_n \leq$ 4000) at 23°C. (● = CIB-PAA)

7.3 The inhibition efficiency of PAAs at 80 °C

Due to the formation of air bubbles at high temperatures which interfere with turbidity measurements; the conductivity measurement was used to evaluate the efficiency of three different concentrations (6, 1.5 and 0.4 ppm) of PAA_s to prevent CaC_2O_4 formation ($[Ca^{2+}]$ = 22 ppm, $[C_2O_4^{2-}]$ = 48 ppm) at 80 °C.

It is worth noting that the conductivity system which was used at 80 °C was the same conductivity system shown in Figure 3.17 (Chapter 3).

7.3.1 Results and Discussion

At the PAA concentration of 6 ppm used at 23 °C, PAA (M_n < 2000 g/mol) with different end groups gave very significant inhibition at 80 °C (Table 7.2), such that in order to discriminate between them it was necessary to reduce the concentration of PAA employed. When this was done at [PAA] = 1.5 and 0.4 ppm, the most effective PAA were found to be the chains terminated by the middle (HIB) hydrophobe. A possible explanation for the reduction in relative effectiveness may lay in the increasingly unfavorable solubilization of these PAA as temperature increases, which may retard transport of the PAA with longer hydrophobes from micelles into solution to interfaces to such an extent that their effective concentration on crystallite surfaces can no longer inhibit growth. Observations of significant foaming in related experiments with HDIB at 100 °C suggest that the surface activity of PAA terminated with the longer alkyl isobutyrates is significant.

The induction time data reported here can be correlated with effects on calcium oxalate hydrate speciation and morphology at 23 °C observed by scanning electron microscopy.[9] Dramatic increases in the amount of COD were observed for polymers with moderately-sized hydrophobic end-groups (HIB and CIB) while shorter and longer hydrophobes gave

predominantly COT. As COT is the phase formed initially according to Ostwald's rule[10] these results suggest adhesion of PAA to the growing crystal surface is weak at this temperature for HIB and CIB end-groups, allowing re-arrangement or re-dissolution to form COD; but strong interactions between the surface and PAA with longer hydrophobic end-groups or fully hydrolysed PAA maintain the initially precipitated calcium oxalate as COT.

Table 7.2- CaC_2O_4 system at 80 °C, $[Ca^{2+}]$ = 22 ppm and $[C_2O_4^{2-}]$ = 48 ppm

End Groups terminated-PAA		M_n	IT (s) by Conductivity		
			6 ppm of PAA	1.5 ppm of PAA	0.4 ppm of PAA
Hydrophilic	CMM	2106	a	a	170 +30 -49
Hydrophobic	EIB	1669	a	a	309 +5 -5
	CIB	1852	a	a	349 +142 -18
	HIB	1981	a	a	452 +180 -86
	DIB	2422	a	324 +117 -52	b
	HDIB	2767	a	292 +121 -12	b

a: indicates that no significant decreasing in conductivity was observed over the 3000 s term of the experiment.

b: indicates that no experiment was performed under this set of conditions.

7.4 Crystal morphologies of CaC_2O_4 in the absence and the presence of PAAs

The crystals of CaC_2O_4 in presence of PAA ($M_n \leq 2000$ g/mol) were collected after 1000 s and filtered through 0.45 μm pore size cellulose acetate filter paper and then characterized by Scanning Electron Microscope.[11] Scale samples were gold-coated and SEM images obtained using a FEI Quanta 200 Environmental SEM at an accelerating voltage of 15 kV.

In experiments carried out at 80 °C, SEM images showed that the crystals of CaC_2O_4 presented in two polymorphs plate-like and aggregation of crystals as clusters for all PAA with different end groups (Figures 7.6, 7.7, 7.8, 7.9, 7.10 and 7.11). Those polymorphs are very similar to the polymorphs of CaC_2O_4 as COM (monoclinic) that was obtained by Doherty at 80 °C (Doherty, 2006).[11] The average length of a plate-like crystal was 12.5, 15.0, 12.5, 12.5, 18.75 and 18.75 in the presence of PAA with end groups CMM, EIB, CIB, HIB, DIB and HDIB respectively. This result is in good agreement with Ostwald's Rule of Stages, which suggests that in most cases the first crystal polymorph to form will be the one which requires the least structural change on proceeding from solution or melt, rather than the polymorph of greatest thermodynamic stability.[10]

Jung et al., (2004)[12] have demonstrated that PAA is very effective in retarding growth on the {121} and {021} faces of COM and slows growth on the {100} faces more effectively than the {010} faces. Mechanistically this is related to the distribution and spacing of the ions on the different surfaces: {010} faces present, mainly oxalate ions, while a dense pattern of calcium ions is presen at {100} faces.[8] Adsorption of PAA to COM nuclei appears to be rapid and irreversible.

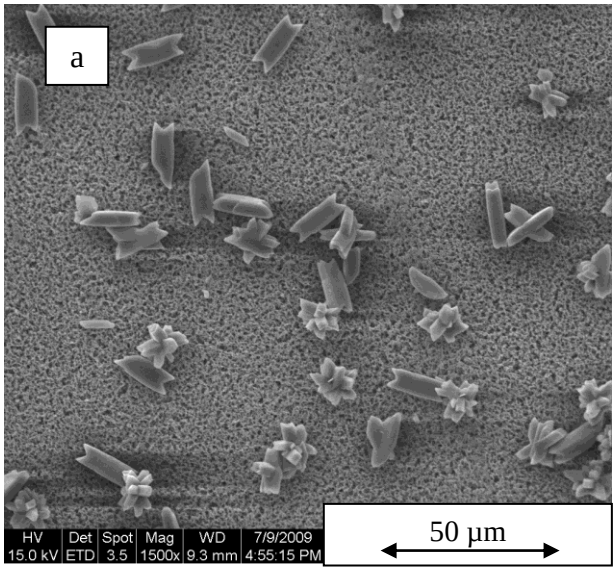

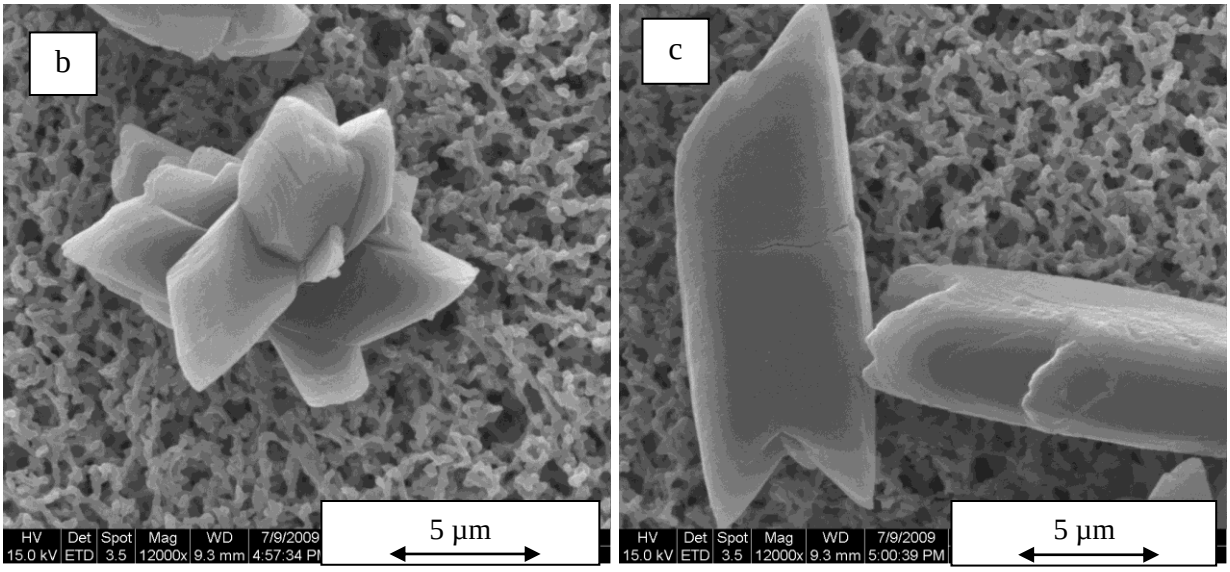

Figure 7.6- Scanning electron micrograph showing (a) a mixture of crystals, (b) aggregation of crystals as clusters morphology and (c) crystal plate-like of calcium oxalate monohydrate crystals in the presence of DIB-PAA (1.5 ppm) at 80 °C.

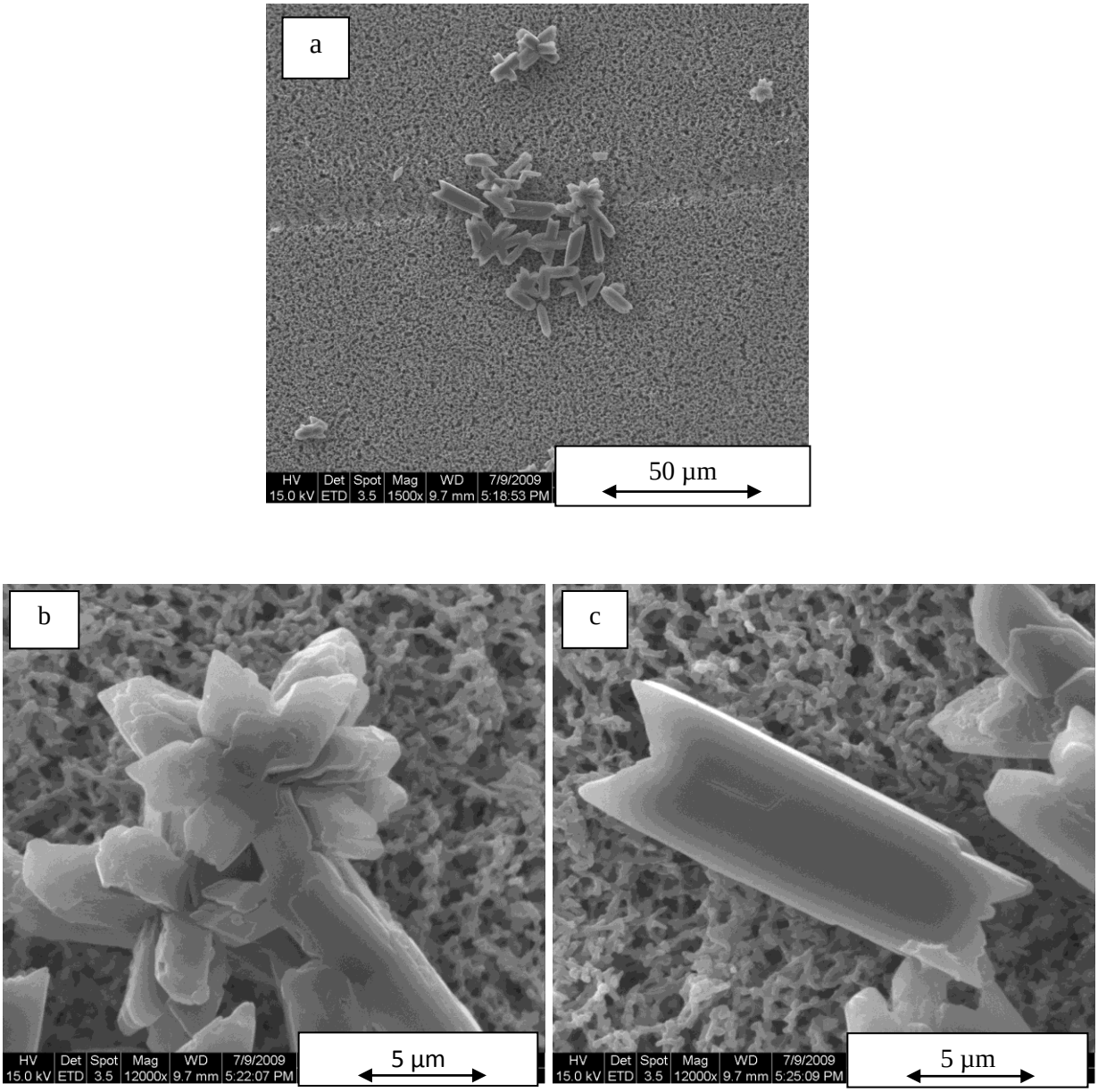

Figure 7.7- Scanning electron micrograph showing (a) a mixture of crystals, (b) aggregation of crystals as clusters morphology and (c) crystal plate-like of calcium oxalate monohydrate crystals in the presence of HDIB-PAA (1.5 ppm) at 80 °C.

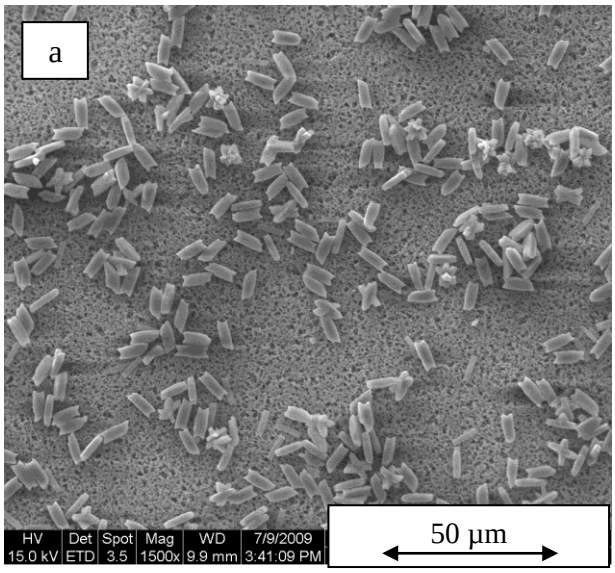

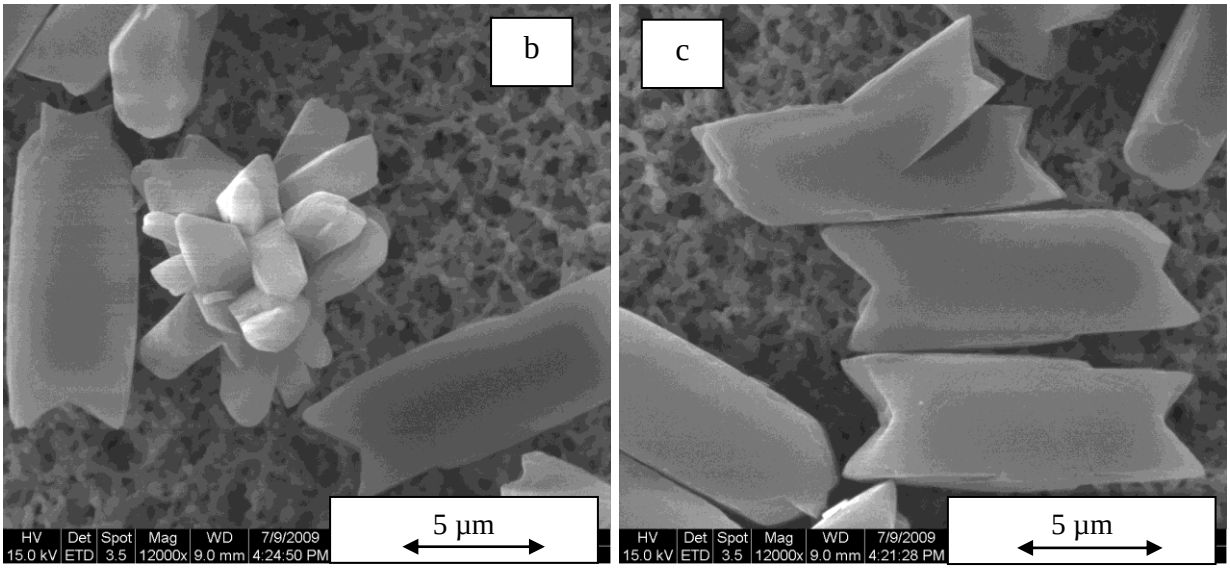

Figure 7.8- Scanning electron micrograph showing (a) a mixture of crystals, (b) aggregation of crystals as clusters morphology and (c) crystal plate-like of calcium oxalate monohydrate crystals in the presence of CIB-PAA (0.4 ppm) at 80 °C.

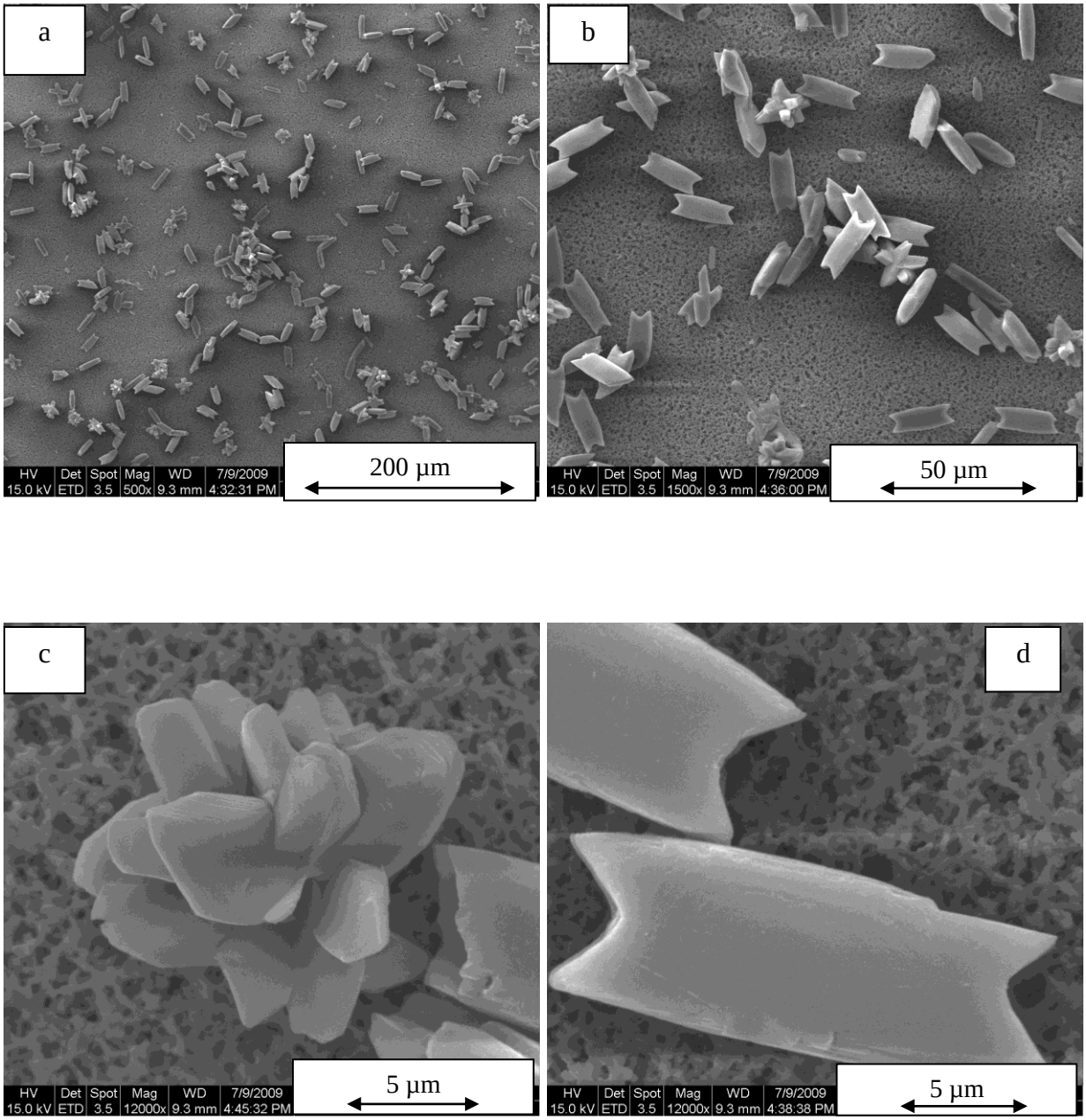

Figure 7.9- Scanning electron micrograph showing (a & b) a mixture of crystals, (c) aggregation of crystals as clusters morphology and (d) crystal plate-like of calcium oxalate monohydrate crystals in the presence of HIB-PAA (0.4 ppm) at 80 °C.

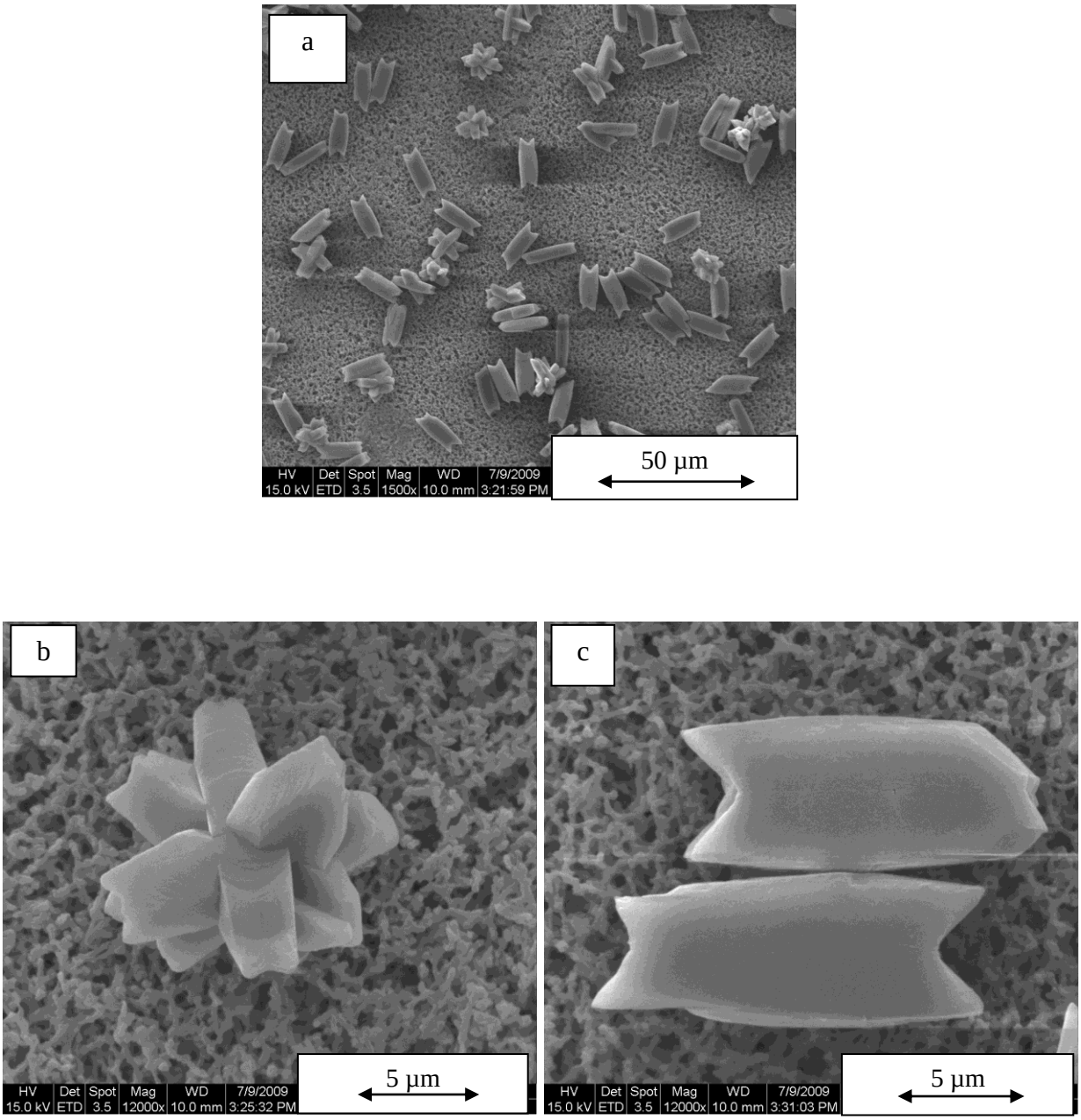

Figure 7.10- Scanning electron micrograph showing (a) a mixture of crystals, (b) aggregation of crystals as clusters morphology and (c) crystal plate-like of calcium oxalate monohydrate crystals in the presence of EIB-PAA (0.4 ppm) at 80 °C.

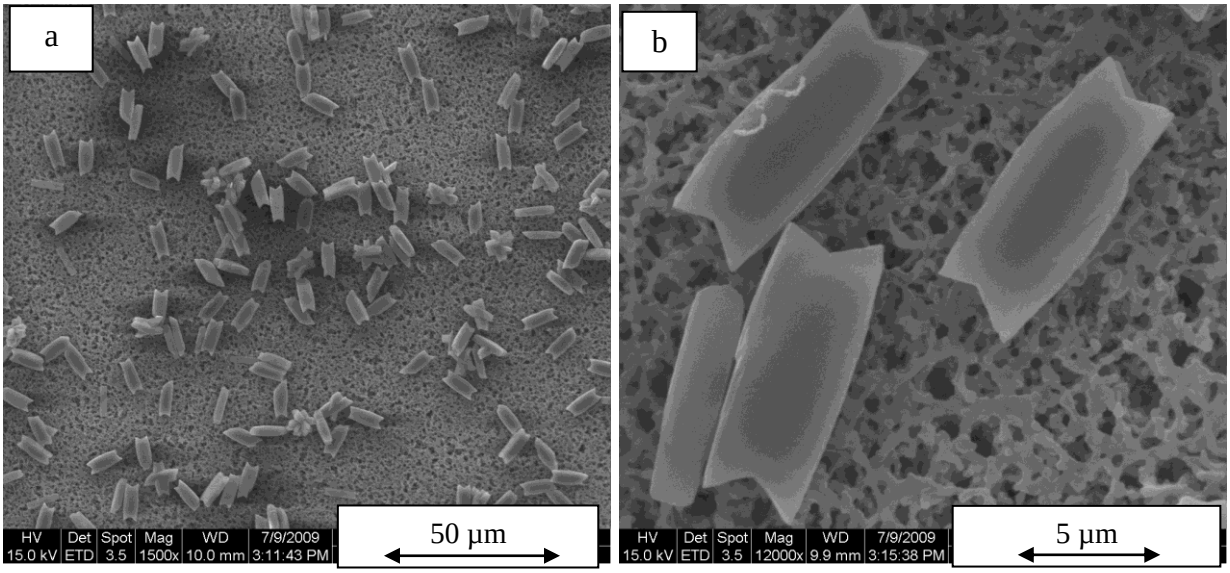

Figure 7.11- Scanning electron micrograph showing (a) a mixture of crystals, (b) crystal plate-like of calcium oxalate monohydrate crystals in the presence of CMM-PAA (0.4 ppm) at 80 °C.

7.5 Conclusion

The effectiveness of PAA scale inhibitors in inhibiting the onset of measurable calcium oxalate precipitation in a model system at room temperature was found to be greatest at molecular masses between 1400 and 3300 g/mol, reproducing earlier findings by Doherty et al. (2004). More significantly, a strong effect of the end-group was found independent of molecular mass, with poly(acrylic acid) terminated with longer hydrophobes such as HDIB or with carboxylic acid end groups showing better performance than chains with intermediate-length hydrophobes in terms of induction time. CIB-PAA inhibitors performed more poorly than HIB-PAA inhibitors, suggesting that association of the hydrophobes as they increase in size is suppressing desorption that would otherwise be encouraged by incorporation of the hydrophobic end-groups. These results were interpreted in terms of the degree to which the scale inhibitors could adsorb to the surface. At 80 °C, the effectiveness of the inhibitors

terminated with short hydrophobes improved, in line with the expected effect of increasing temperature on surfactant solubility, but the effectiveness of the inhibitors terminated with long hydrophobes declined, which was provisionally attributed to micellization phenomena retarding transport of polymer through the aqueous phase and preventing sufficient coverage of active sites on the crystal surfaces. These results are in good accordance with the results obtained for other scaling minerals in Chapters 3, 5 and 6.

References

1. Senogles, E.; Doherty, W. O. S.; Crees, O. L., Scale Inhibitors, Polymeric. In *Encyclopedia of Polymer Science and Technology*, 2nd ed.; Kroschwitz, J., Ed. Wiley-Interscience: Boca Raton, 1996; pp 7587-7594.

2. Batstone, D. B. In *Scale Alleviation Trials, 1970*, 38th conference of Australian Sugar Cane Technologists, 1971; 1971; pp 207-210.

3. Doherty, W. O. S.; Crees, O. L.; Senogles, E. *Cryst. Res. Technol.* **1995,** 30, (6), 791-800.

4. Clarke, S. J. *Proc. Aust. Soc. Sugar Cane Technol.* **1989,** 11.

5. Doherty, W. O. S.; Fellows, C. M.; Gorjian, S.; Senogles, E.; Cheung, W. H. *Journal of Applied Polymer Science* **2004,** 91, (3), 2035-2041.

6. Steel, R. G.; Torrie, J. H., *Principles and procedures of statistics*. 2 nd ed.; McGraw-Hill, Inc.: New York, 1980.

7. Binglin, Y. *Water Treatment* **1989,** 4, 257-265.

8. Tunik, L.; Addadi, L.; Garti, N.; Furedi-Milhofer, H. *J. Cryst. Growth* **1996,** 167, 748.

9. East, C. P.; Wallace, A. D.; Al-Hamzah, A.; Doherty, W. O. S.; Fellows, C. M. *Journal of Applied Polymer Science* **2010,** 115, (4), 2127-2135.

10. De Yoreo, J. J.; Vekilov, P. G., Principles of Crystal Nucleation and Growth In *Reviews in Mineralogy and Geochemistry* Mineralogical Society of America: Washington, DC, 2003; Vol. 54, pp 57-93.

11. Doherty, W. O. S. *Ind. Eng. Chem. Res.* **2006,** 45, 642-647.

12. Jung, T.; Sheng, X.; Choi, C. K.; Kim, W.-S.; Wesson, J. A.; Ward, M. D. *Langmuir* **2004,** 20, 8587.

CHAPTER EIGHT

Summary

8.1 Summary

Polyelectrolytes or polyions such as PAA which contain hydrophobic end groups are called associating poly-electrolytes or polysoaps. The associating poly-electrolyte can self-assemble to form intermolecular structures such as, micelles, vesicles and bilayers. As the amount of hydrophobic end group to polymer is increased by longer hydrophobic end group, the critical polymer concentration (CPC) for polysoap behavior will decrease. Polysoap behavior is local micelles in water for poly electrolyte with hydrophobic end group that have more than nine carbon atoms. [1]

In this study, a number of polyacrylic acids (PAA) with different length of hydrophilic and hydrophobic end groups (number of carbon atoms 4 to 20) and molecular mass (1400 to 17000 g/mol) were used to prevent different scale crystallizations such as calcium carbonate ($CaCO_3$), calcium oxalate (CaC_2O_4), calcium sulfate ($CaSO_4$) and magnesium hydroxide ($Mg(OH)_2$). The results showed that the most effectiveness of molecular mass of PAA with different end groups was $M_n \leq 2000$ g/mol. [2, 3] The end groups of PAA also played a significant role in inhibition efficiency, induction time and the morphology of crystals. In most conditions, the low molecular mass PAA with hydrophobic mid-length end group (n-hexyl isobutryate, HIB) had the highest inhibition efficiency and longest induction time as shown in Figure 8.1. Investigation of the efficiency of these new scale inhibitors to retard the alkaline and hard scales in pilot desalination plant is recommended for future work.

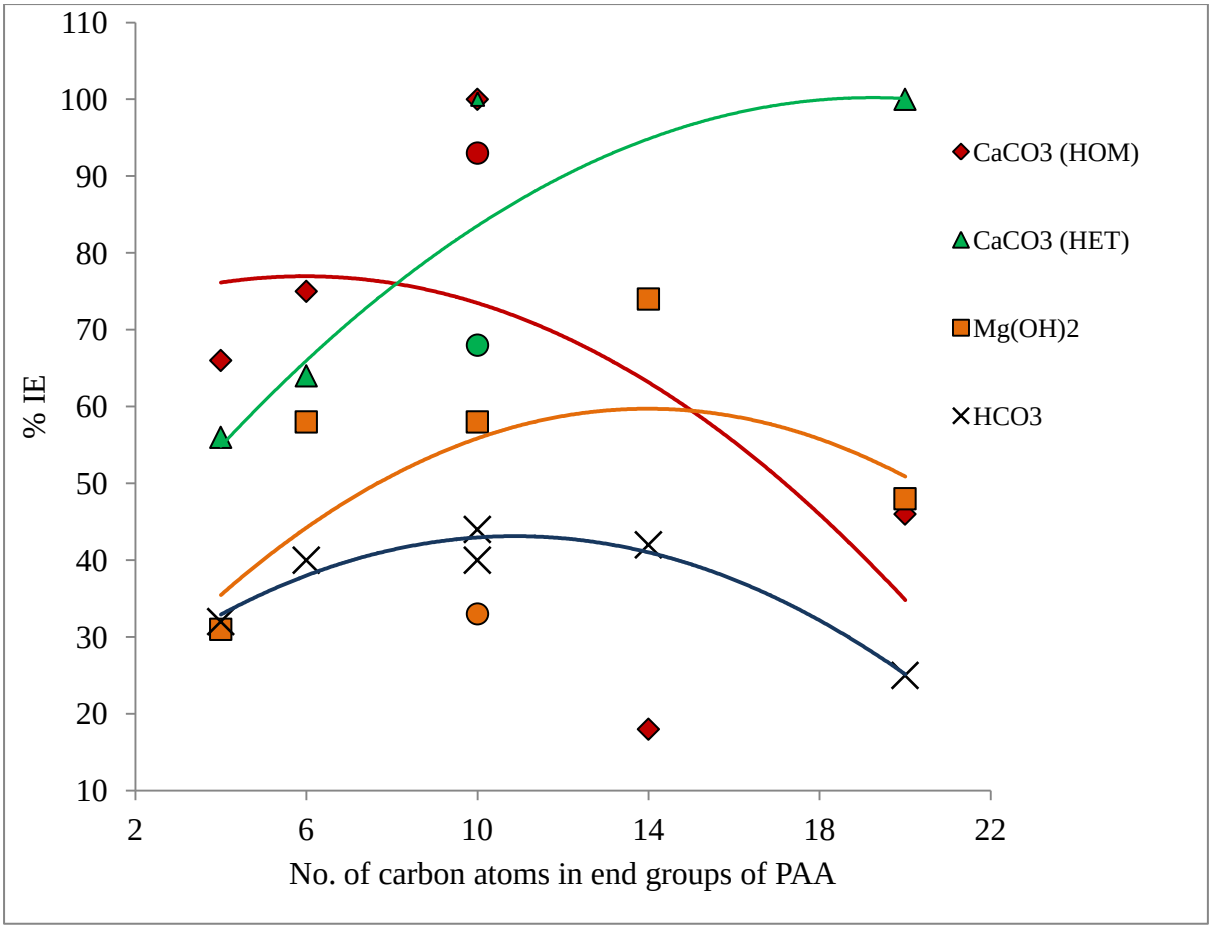

Figure 8.1- The effect of end groups of PAA ($M_n \leq 2000$ g/mol) in inhibition efficiency for deposition of different scales at 100 °C. (● with different colors = CIB), ♦HOM noted homogenous crystallization of $CaCO_3$, ▲ HET noted heterogeneous crystallization of $CaCO_3$, × noted thermal decomposition of HCO_3^- and ▢ noted the formation of $Mg(OH)_2$.

The role of end groups of PAA to inhibit scale formation may be very significant in encouraging PAA chains to adsorb in the active face of growth crystals, modifying crystal habit and retarding growth. The rates of adsorption/desorption are very important for achieving a high inhibition of scale formation. Therefore, more rapid and less reversible adsorption of PAA to delay the crystal growth will be more required. This can be achieved by

the hydrophobic end groups and is very dependent on the length of the hydrophobe, particularly at high temperatures.

A clear example for the effect of length and shape of end group is middle hydrophobic end groups (cyclohexyl isobutrate, CIB & HIB). Both end groups contain the same number of carbon atoms however; its shape is different. The efficiency of PAA with the two end groups in most cases was different with HIB-PAA always showing better efficiency than CIB-PAA at equivalent molecular mass.

Another effect of hydrophobic end group is a self-association to form the micelles in solution. A good example in this study for this case is PAA with the longest hydrophobic end group (hexadecyl isobutyrate, HDIB). A low molecular mass of HDIB-PAA (M_n = 1687 g/mole) had a highest ratio (0.187) of hydrophobe to polyelectrolyte mass making that polymer very surface active. That phenomenon appears clearly in an excellent inhibition of the heterogenous crystallization of $CaCO_3$ at 100 °C. This result may lead to the development of new scale inhibitors with high performance to inhibit crystallization on surfaces

The activity coefficients of HCO_3^-, CO_3^{2-}, OH^-, Ca^{2+}, Mg^{2+} and CO_2 (aq) at 25 °C and 100 °C at pH = 8.1 and 9.0 were estimated using the Pitzer [4, 5] equations and then used to calculate ΔG of the competitive reactions for both the unimolecular mechanism [6] and bimolecular mechanism [7] at those conditions. The results showed that, both the mechanisms were in effect. At low temperature the bimolecular mechanism is likely to predominate, however at high temperature (T > 80 °C) the unimolecular mechanism was predominant. The result indicated that the alkaline scale formation in thermal desalination plant is thermodynamically controlled.

The rate coefficient of thermal decomposition of HCO_3^- at 97.2 °C in the absence and presence of 10 ppm of PAA with different end groups and molecular mass was determined.

Both end groups and molecular mass of PAA were found to play an important role. For all end groups of PAA except HDIB-PAA, the rate coefficient of thermal decomposition of 40 ppm HCO_3^- increased with increasing molecular mass. The mechanism of the thermal decomposition of HCO_3^- in the presence of PAA with different end groups and molecular mass was suggested. That mechanism based on preventing heterogeneous decomposition of HCO_3^- on the interface surfaces such as the water/air interface of bubbles that form in bulk solution and the interface surface of round bottom flask. The surrounding of bubbles by PAAs may increase with decreasing molecular mass and increasing mobility of PAA. Further work remains to be done to understand the mechanism of inhibition of thermal decomposition of HCO_3^- in the presence of PAA, as well as for determining the surface tension for PAA solutions.

An intrinsic exposed core optical fibre sensor (IECOFS) was developed to study the heterogeneous crystalillzation of $CaCO_3$ and coprecipitation of $CaCO_3$ and $CaSO_4$ at 100-120 °C in the absence and presence of low molcular mass ($M_n \leq 2000$ g/mol) PAA with different end groups. 6.7 ppm of HIB-PAA and HDIB-PAA showed excellent inhibition efficiency in preventing the hetrogeneous deposit of $CaCO_3$ at 100 °C. Low molecular mass ($M_n \leq 2000$ g/mol) PAA (10 ppm) with different end groups showed a very siginificant inhibition of hetrogeneous coprecipitation of $CaCO_3$ and $CaSO_4$ at 120 °C. Further work remains to be carried out in terms of mechanism and morphology for the heterogeneous crystalillzation of $CaCO_3$ and coprecipitation of $CaCO_3$ and $CaSO_4$ in the presence of PAA at high temperatures.

Most previous studies have only focused on the effect of the molecular mass of scale inhibitor in the prevention and retardation of the formation of different scales. The results in this study for the effectiveness of the end groups open wide the synthesis and study of new polymeric scale inhibitors with specific architecture and high efficiency. Controlled methods

of living radical polymerization such as nitroxide-mediated polymerization (NMP), atomic transfer radical polymerization (ATRP) and radical addition-fragmentation chain transfer (RAFT) polymerization may be good options to achieve that target. These methods allow us to synthesize and develop novel polymer as scale inhibitors with low polydispersity and advanced properties to prevent scale formation.

References

1. Kotz, J.; Kosmella, S.; Beitz, T. *Prog. Polym. Sci* **2001,** 26, 1199-1232.

2. Amjad, Z. *J. Colloid Interf. Sci.* **1988,** 123, (2), 523-536.

3. Amjad, Z., Scale Inhibition in Desalination Application: an overview. In *Reviews on Corrosion Inhibitor Science and Technology*, Denver, 1996; Vol. 2.

4. Millero, F.; Huang, F.; Graham, T.; Pierrot, D. *Geochim. Cosmochim Ac.* **2007,** 71, (1), 46-55.

5. Millero, F.; Pierrot, D. *Aquat. Geochem.* **1998,** 4, 153-199.

6. Dooly, R.; Glater, J. *Desalination* **1972,** 11, (1), 1-16.

7. Langelier, W. F.; Caldwell, D. H.; Lawrence, W. B.; Spaulding, C. H. *J. Ind. Eng. Chem.* **1950,** 42, 126-30.

Appendix 1

A1.1 Pitzer model for calcium sulfate hemihydrate ($CaSO_4.1/2\ H_2O$)

In thermal desalination, calcium sulfate exists in three forms: calcium sulfate dihydrate or gypsum ($CaSO_4.2H_2O$, calcium sulfate hemihydrate ($CaSO_4.1/2\ H_2O$) and calcium sulfate anhydrite ($CaSO_4$). Under supersaturation conditions of calcium sulfate, the temperature of brine solution may control the precipitation form. For example, below 100 °C the predominant forms are $CaSO_4.2H_2O$ and $CaSO_4$, however $CaSO_4.1/2\ H_2O$ dominates above 102°C as shown in Figure 1.6 in Chapter 1. [1, 2]

Calcium sulfate deposit is very hard, adherent and difficult and costly to remove mechanically. Most MSF plants currently operate at a top brine temperature (TBT) under 122 °C to keep brine solution under supersaturation in respect to calcium sulfate ($CaSO_4.1/2\ H_2O$ and $CaSO_4$) formation.

Recently, a hybrid desalination process using a combination of nanofiltration NF as seawater pre-treatment (to reduce the concentration of some ions e.g. SO_4^{2-} and Ca^{2+}) with MSF (NF-MSF) to increase TBT upon 140 °C was proposed by Hamed *et. al.*(2005).[3] Application of this process requires knowledge of the thermodynamics of solubility product K_{sp} for $CaSO_4.1/2\ H_2O$ (Eq- A1.1) at different temperatures and total dissolved solid (TDS) to control its formation by keeping the brine solution under supersaturation which make that process more economic. The solubilities of $CaSO_4.1/2\ H_2O$ at different temperatures and TDS were studied by Zannoni, *et. al.,* (1987)[4] and for more benefit from their data for using in normal and hybrid desalination applications the K_{sp} (Eq- A1.1) for $CaSO_4.1/2\ H_2O$ should be calculated.

$$K_{sp} = \gamma_{Ca^{2+}} [Ca^{2+}] \times \gamma_{SO_4^{2-}} [SO_4^{2-}] \times (a_{H2O})^{0.5} \qquad \text{Eq- A1.1}$$

Where, a_{H2O} is the activity of H_2O, and γ_{Ca}^{2+} and γ_{SO4}^{2-} are the activity coefficient of Ca^{2+} and SO_4^{2-} respectively.

The Pitzer model (explained in Chapter 1) was used to calculate the activity of H_2O and activity coefficient of Ca^{2+} and SO_4^{2-} at different temperatures and TDS as follows

$$ln\,(\gamma\,(Ca^{2+})) =$$

$$4f^{\gamma} + 2m_{Cl}\left(B_{CaCl_2} + m_{Na}C_{CaCl_2}\right) + 4m_{Na}\,m_{Cl}\,B'_{NaCl} + 2m_{Na}\,m_{Cl}\,\mathrm{C_{NaCl}} +$$

$$\mathrm{m_{Na}}\,(\,2\theta_{\mathrm{NaCa}} + \mathrm{m_{Cl}}\,\psi_{\mathrm{Na-Ca-Cl}}) \qquad \text{Eq- A1.2}$$

$$ln\,(\gamma\,(SO_4^{2-})) = 4f^{\gamma} + 2m_{Na}\left(B_{Na_2SO_4} + m_{Cl}C_{Na_2SO_4}\right) + 4m_{Na}\,m_{Cl}\,B'_{NaCl} +$$

$$2m_{Na}\,m_{Cl}\,\mathrm{C_{NaCl}} + \mathrm{m_{Cl}}\left(\,2\theta_{\mathrm{Cl-SO_4}} + \mathrm{m_{Na}}\,\psi_{\mathrm{Cl-SO4-Na}}\right) \qquad \text{Eq- A1.3}$$

The activity of water in equation 5.1 was estimated as explained in Chapter 1 (Eq-1.25)

A1.2 The values of Pitzer parameters for ionic strength dependence (B_{MX}, B'_{MX} and C_{MX}) for NaCl as 1:1 electrolyte and Na_2SO_4 and $CaCl_2$ as 2:1 electrolytes in Eqs. A1.2 and A1.3 are given as follows:

$$B_{MX} = \beta^{\circ}_{MX} + \left(\frac{\beta^{1}_{MX}}{2I}\right)[1 - (1 + 2I^{0.5})\exp(-2I^{0.5})] \qquad \text{Eq- A1.4}$$

$$B'_{MX} = \left(\frac{\beta^{1}_{MX}}{2I^{2}}\right)[-1 + (1 + 2I^{0.5} + 2I\exp(-2I^{0.5})] \qquad \text{Eq- A1.5}$$

$$C_{MX} = \frac{C^{\phi}_{MX}}{(2|Z_M Z_X|^{0.5})} \qquad \text{Eq- A1.6}$$

$$B^{\emptyset}_{NaCl} = \beta^{\circ}_{NaCl} + \beta^{1}_{NaCl}\,exp(-2I^{0.5}) \qquad \text{Eq- A1.7}$$

And f^{γ} in Eqs. (5.2 and 5.3) is Debye-Hückel term as follows

$$\int^{\gamma} = -A_{\phi}\left[\frac{I^{0.5}}{(1+1.2I^{0.5})} + \frac{2}{1.2}\ln(1+1.2I^{0.5})\right] \quad \text{Eq- A1.8}$$

A1.3- Pitzer coefficient values temperature dependent ($\boldsymbol{\beta^{(0)}_{NaCl}}$, $\boldsymbol{\beta^{(1)}_{NaCl}}$ and $\boldsymbol{C^{\phi}_{NaCl}}$) for NaCl and $CaCl_2$ are given by in Eq-A1.9.

$$P(T) = a_1 + a_2T + \frac{a_3}{T} + a_4 \ln T + \frac{a_5}{T-263} + a_6T^2 + \frac{a_7}{680-T} + \frac{a_8}{T-227} \quad \text{Eq-A1.9}$$

Where, *P* equal to ($\beta^{(O)}_{NaCl}$, $\beta^{(1)}_{NaCl}$ *and* C^{ϕ}_{NaCl})

The values of parameters a_1, a_2, a_3, a_4, a_5, a_6, a_7 *and* a_8 for NaCl and $CaCl_2$ are given by Møller, 1988[5] and Greenberg and Møller, 1989 [6] from 0 - 250 °C (Tables A1.1 and A1.2).

Table A1.1- Pitzer coefficient for NaCl

parameter	$\beta^{(O)}_{NaCl}$	$\beta^{(1)}_{NaCl}$	C^{ϕ}_{NaCl}
a_1	14.37832	-0.483060685	-0.100588714
a_2	5.6077×10^{-3}	1.4067747×10^{-3}	-1.8052981×10^{-5}
a_3	-422.185236	119.311989	8.61185543
a_4	-2.51227	0.0	0.012488095
a_5	0.0	0.0	0.0
a_6	$-2.61718135\times 10^{-6}$	0.0	3.41172108×10^{-8}
a_7	4.43854508	0.0	0.0683040995
a_8	-1.70502337	-4.23433299	0.293922611

Table A1.2- Pitzer coefficient for $CaCl_2$

parameter	$\beta^{(O)}_{CaCl_2}$	$\beta^{(1)}_{CaCl_2}$	$\beta^{(2)}_{CaCl_2}$	$C^{\phi}_{CaCl_2}$
a_1	-94.1895832	3.4787	0.0	19.305560024
a_2	$-4.047500526\times 10^{-2}$	-1.5417×10^{-2}	0.0	9.77090932×10^{-3}
a_3	2345.50368	0.0	0.0	-428.383748
a_4	17.09123	0.0	0.0	-3.579966343
a_5	-0.92288584	0.0	0.0	8.82068538×10^{-2}
a_6	1.51488122×10^{-5}	3.1791×10^{-5}	0.0	$-4.62270238\times 10^{-6}$
a_7	-1.39082	0.0	0.0	9.91113465
a_8	0.0	0.0	0.0	0.0

A1.4 Pitzer coefficient values for temperature dependence

The Pitzer coefficient values for temperature dependence, $(\beta^{(O)}_{Na_2SO_4}, \beta^{(1)}_{Na_2SO_4} \text{ and } C^{\phi}_{Na_2SO_4})$ for Na_2SO_4 are given by Eq-A1.10

$$P = a + b\left(\frac{1}{T} - \frac{1}{298.15}\right) + c\ln\left(\frac{T}{298.15}\right) \qquad \text{Eq- A1.10}$$

The value of parameters *a, b* and *c* of Na_2SO_4 available in references (e.g. Pierrot, et. al. (1997)[7] & Millero and Pierrot, (1998)[8] are only valid until 100 °C. Moreover, most references only present accurate values of $(\beta^{(O)}_{Na_2SO_4}, \beta^{(1)}_{Na_2SO_4} \text{ and } C^{\phi}_{Na_2SO_4})$ at 25 °C (Sheikholeslami & Ong, 2003)[9] and Neck, *et al.*, (1997), although values at 25, 50, 100 and 150 °C are

presented in Pitzer (1986). In this study, the values of parameters *a, b* and *c* for Pitzer coefficient temperature dependence ($\beta^{(O)}_{Na_2SO_4}$, $\beta^{(1)}_{Na_2SO_4}$ and $C^{\phi}_{Na_2SO_4}$) of Na_2SO_4 were estimated based on the accurate values at 25, 100 and 150 °C presented in Pitzer (1986) to extend their validity over a wider range of temperature and calculate absolute values at the temperatures of interest (112, 124, 136 and 148 °C).

The parameter *a* is temperature independent (Eq- A1.10), therefore its value is equal to the value of ($\beta^{(O)}_{Na_2SO_4}$, $\beta^{(1)}_{Na_2SO_4}$ and $C^{\phi}_{Na_2SO_4}$) at 25 °C given by Pitzer (1986). The parameters *b* and *c* can be estimated by the substitution value of ($\beta^{(O)}_{Na_2SO_4}$, $\beta^{(1)}_{Na_2SO_4}$ and $C^{\phi}_{Na_2SO_4}$) at certain T in Eq- A1.10.

For example, the parameters *b* and *c* of $\beta^{(1)}_{Na_2SO_4}$ at 100 and 150 °C can be estimated by using Eq- A1.10 and its values at these temperatures as follows:

At 25 °C $\beta^{(1)}_{Na_2SO_4} = 1.0559$, (*a* value)

At 100 °C,

$\beta^{(1)}_{Na_2SO_4} = 1.3421$, by substitution Eq- A1.10

$$1.3421 = 1.0559 + b\left(\frac{1}{373.15} - \frac{1}{298.15}\right) + c\ln\left(\frac{373.15}{298.15}\right) \qquad \text{Eq- A1.11}$$

At 150 °C,

$\beta^{(1)}_{Na_2SO_4} = 1.5710$

$$1.5710 = 1.0559 + b\left(\frac{1}{423.15} - \frac{1}{298.15}\right) + c\ln\left(\frac{423.15}{298.15}\right) \qquad \text{Eq- A1.12}$$

b and *c* can be determined by solving Eq- A1.11 and Eq- A1.12.

The values of parameters *a, b* and *c* of ($\beta^{(O)}_{Na_2SO_4}$, $\beta^{(1)}_{Na_2SO_4}$ and $C^{\phi}_{Na_2SO_4}$) are tabulated in Table A1.3. The comparison between values of ($\beta^{(O)}_{Na_2SO_4}$, $\beta^{(1)}_{Na_2SO_4}$ and $C^{\phi}_{Na_2SO_4}$) calculated in this study and their values in Pitzer (1986) are tabulated in Table A1.4 at 100 and 150 °C covering the temperature range of interest to this study.

Table A1.3- Values of parameters *a, b* and *c* for Pitzer coefficient temperature dependence ($\beta^{(O)}_{Na_2SO_4}$, $\beta^{(1)}_{Na_2SO_4}$ and $C^{\phi}_{Na_2SO_4}$) of Na_2SO_4.

parameter	$\beta^{(O)}_{Na_2SO_4}$	$\beta^{(1)}_{Na_2SO_4}$	$\beta^{(2)}_{Na_2SO_4}$	$C^{\phi}_{Na_2SO_4}$
a	0.0181	1.0559	0.0	0.00202
b	-125.284	1122.64	0.0	23.602
c	0.00152653	4.64838	0.0	0.0438

Table A1.4- The comparison between the values of ($\beta^{(O)}_{Na_2SO_4}$, $\beta^{(1)}_{Na_2SO_4}$ and $C^{\phi}_{Na_2SO_4}$) which was calculated in this study and their values in K. Pitzer (1986) at 100 and 150 °C.

Pitzer coefficient temperature dependent	This study		Values from K. Pitzer (1986)	
	100 °C	150 °C	100 °C	150 °C
$\beta^{(O)}_{Na_2SO_4}$	0.1029	0.1427	0.1029	0.1227
$\beta^{(1)}_{Na_2SO_4}$	1.3421	1.5711	1.3421	1.5710
$C^{\phi}_{Na_2SO_4}$	-0.0041	-0.0060	-0.0041	-0.0060

The values of terms θ_{ij} and Ψ_{ijk} in Eq- A1.2 and A1.3 are given in Millero, F, and Pierrot, D., 1998 as shown in Table A1.5.

Table A1.5- The values of terms θ_{ij} and Ψ_{ijk}

i	j	k	θ_{ij}	Ψ_{ijk}
Na	Ca	Cl	0.07	-0.007
Na	Cl	SO_4	0.07	-0.055

A1.5 Result

The results for estimation of activity coefficient (γ) of Ca^{2+} and SO_4^{2-} and K_{sp} of $CaSO_4.1/2H_2O$ showed, the values of γ and K_{sp} decreasing with increasing temperature (from 100 to 148 °C) and TDS (form 63000 to 99000 mg/L) as shown in Table A1.6 and Figure A1.1.

In thermal desalination such as MSF and the new approach by hybrid NF-MSF, the goal should be to keep the brine solution under supersaturation in respect to $CaSO_4.1/2\ H_2O$ formation to make that approach more economic at certain conditions like TDS and temperature. For example, the ion product (Q_{IP}) of $CaSO_4.1/2\ H_2O$ at 1.4 concentration factor (CF, TDS = 63000 mg/L) at different temperatures was calculated using Eq-A1.1 based on the concentration of Ca^{2+} and SO_4^{2-} proposed by Zannoni, *et al.*, (1987)[4] and activity of H_2O and activity coefficient of Ca^{2+} and SO_4^{2-} obtained by this study. The results showed that, the given brine solutions are under supersaturation in respect to $CaSO_4.1/2\ H_2O$ formation at 100 and 112 °C (Q_{IP} / K_{sp} = 0.52 and 0.79 respectively) as shown in Table A1.7. However, with increasing temperature to 124 °C the ratio of Q_{IP} /K_{sp} increases to 1.22 which indicates the brine solution (at those conditions) is at supersaturation stage and precipitation of $CaSO_4.1/2$

H_2O is favoured. With increasing temperature to 136 and 148 °C, the ratio of Q_{IP} /K_{sp} increase to 1.95 and 3.20 respectively indicating to the inverse solubility of $CaSO_4.1/2\ H_2O$ with increasing temperature. These results agree well with the $CaSO_4.1/2\ H_2O$ formation in MSF desalination plant where the $CaSO_4.1/2\ H_2O$ appears over 122 °C.[10]

Table A1.6- The activity of H_2O, activity coefficient of Ca^{2+} and SO_4^{2-} and k_{sp} for $CaSO_4.1/2\ H_2O$ at different temperatures and TDS (Zannoni, *et. al.*, (1987)[4]

TDS	63000	67500	72000	76500	81000	81500	90000	94500	99000
Ca ppm	1413	1513	1614	1715	1816	1917	2018	2119	2220
				T = 100 °C					
SO_4 ppm	9541	8759	8075	7471	6933	6451	6017	5623	5265
a(H_2O)	0.9553	0.9517	0.9480	0.9442	0.9404	0.9364	0.9324	0.9284	0.9242
γ (Ca^{2+})	0.119	0.117	0.115	0.114	0.112	0.111	0.110	0.110	0.109
γ (SO_4^{2-})	0.055	0.052	0.049	0.047	0.044	0.042	0.040	0.039	0.037
K_{sp} ×10^{-5}	2.26	1.93	1.66	1.44	1.26	1.11	0.981	0.871	0.777
				T = 112 °C					
SO_4 ppm	6315	5798	5345	4945	4589	4270	3983	3722	3485
a(H_2O)	0.9590	0.9559	0.9527	0.9495	0.9462	0.9429	0.9395	0.9361	0.9327
γ (Ca^{2+})	0.097	0.095	0.093	0.092	0.090	0.089	0.089	0.088	0.087
γ (SO_4^{2-})	0.056	0.054	0.051	0.049	0.047	0.045	0.043	0.041	0.039
K_{sp} ×10^{-5}	1.25	1.15	1.06	0.989	0.922	0.863	0.810	0.761	0.716
				T = 124 °C					
SO_4 ppm	4086	3735	3443	3185	2956	2750	2565	2397	2245
a(H_2O)	0.9594	0.9562	0.9531	0.9499	0.9467	0.9434	0.9401	0.9367	0.9333
γ (Ca^{2+})	0.102	0.100	0.098	0.097	0.095	0.094	0.093	0.092	0.091
γ (SO_4^{2-})	0.046	0.044	0.041	0.039	0.037	0.035	0.034	0.032	0.031
K_{sp} ×10^{-6}	7.01	6.38	5.85	5.39	4.98	4.62	4.30	4.00	3.74

T = 136 °C									
SO_4 ppm	2550	2341	2158	1997	1853	1724	1608	1503	1407
a(H_2O)	0.9597	0.9566	0.9535	0.9504	0.9472	0.9439	0.9407	0.9373	0.9340
γ (Ca^{2+})	0.094	0.092	0.090	0.088	0.087	0.085	0.084	0.083	0.082
γ (SO_4^{2-})	0.042	0.039	0.037	0.035	0.033	0.032	0.030	0.029	0.028
K_{sp} ×10^{-6}	3.64	3.08	2.63	2.26	1.96	1.71	1.50	1.33	1.17
T = 148 °C									
SO_4 ppm	1556	1428	1316	1218	1130	1052	981	917	858
a(H_2O)	0.9601	0.9571	0.9540	0.9509	0.9477	0.9445	0.9413	0.9380	0.9347
γ (Ca^{2+})	0.086	0.084	0.082	0.080	0.078	0.077	0.076	0.075	0.073
γ (SO_4^{2-})	0.038	0.035	0.033	0.032	0.030	0.028	0.027	0.026	0.025
K_{sp} ×10^{-6}	1.82	1.53	1.31	1.12	0.968	0.842	0.737	0.648	0.572

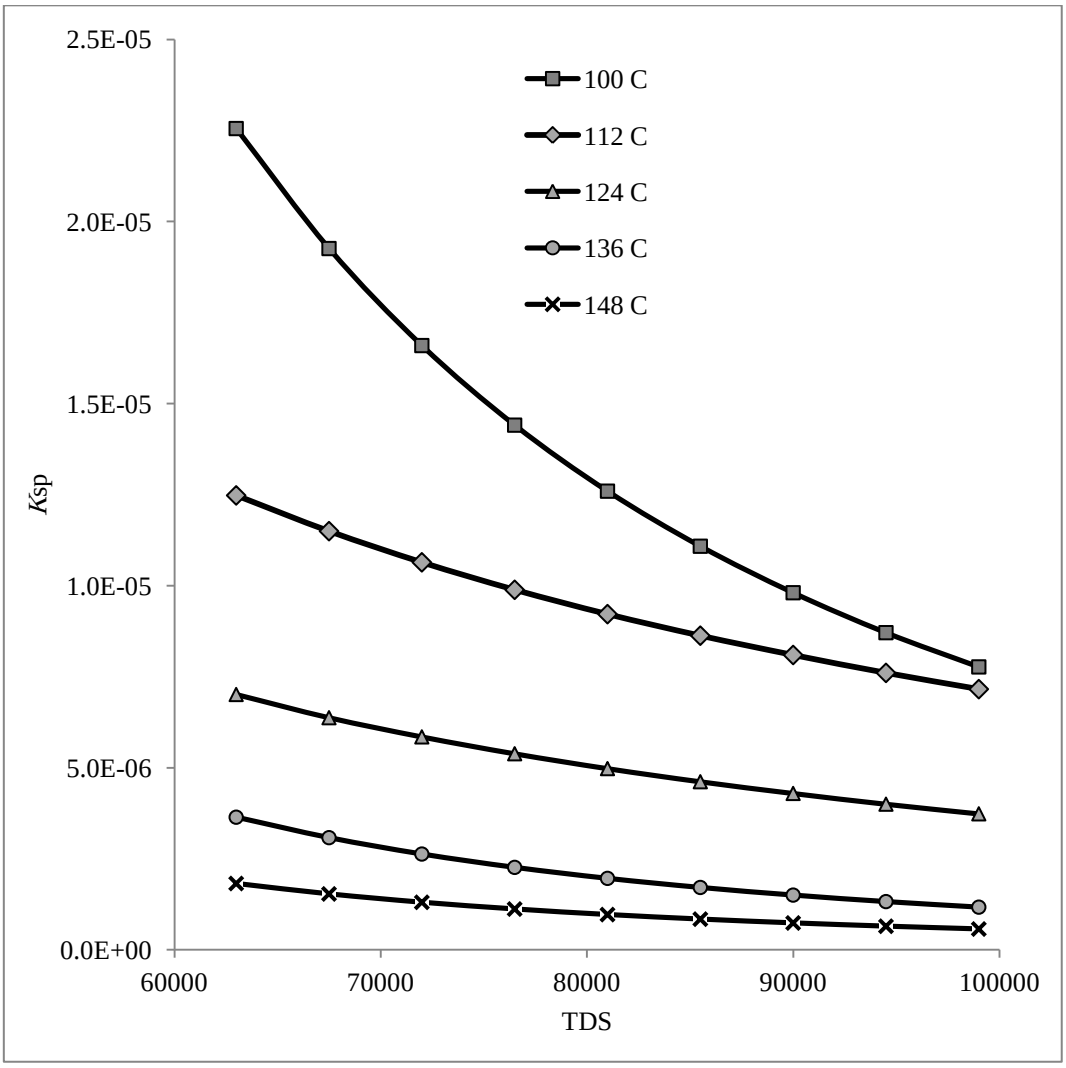

Figure A1.1- k_{sp} for $CaSO_4.1/2\ H_2O$ at different temperatures and TDS

Table A1.7- Ion product (Q_{IP}) and K_{sp} for $CaSO_4.1/2\ H_2O$ at different temperatures and 1.4 concentration factor (CF), TDS= 63000 mg/L

Temp. °C	Q_{IP}	K_{sp}	Q_{IP} / K_{sp}
100	1.18×10^{-5}	2.26×10^{-5}	0.52
112	9.83×10^{-6}	1.25×10^{-5}	0.79
124	8.53×10^{-6}	7.01×10^{-6}	1.22
136	7.10×10^{-6}	3.64×10^{-6}	1.95
148	5.82×10^{-6}	1.82×10^{-6}	3.20

References

1. Shams El Din, A. M.; El-Dahshan, M. E.; Mohammed, R. A. *Desalination* **2005,** 177, (1-3), 241-258.

2. Sheikholeslami, R. *Desalination* **2003,** 154, (2), 117-127.

3. Hamed, O. A. *Desalination* **2005,** 186, (1-3), 207-214.

4. Zannoni, R.; Resini, I.; Liberti, L.; Santori, M.; Boari, G. *Desalination* **1987,** 66, 431-442.

5. Møller, N. *Geochim. Cosmochim. Ac.***1988,** 52, (4), 821-837.

6. Greenberg, J. P.; Møller, N. *Geochim. Cosmochim. Ac.* **1989**

53, (10).

7. Pierrot, D.; Millero, F.; Roy, L. N.; Roy, R. N.; Doneski, A.; Niederschmidt, J. *J. Solution Chem* **1997,** 26, 31-45.

8. Millero, F.; Pierrot, D. *Aquat. Geochem.* **1998,** 4, 153-199.

9. Sheikholeslami, R.; Ong, H. W. K. *Desalination* **2003,** 157, (1-3), 217-234.

10. Al-Sofi, M. A. *Desalination* **1999,** 126, 61-76.